

Nanoscale

Accepted Manuscript



This is an *Accepted Manuscript*, which has been through the Royal Society of Chemistry peer review process and has been accepted for publication.

Accepted Manuscripts are published online shortly after acceptance, before technical editing, formatting and proof reading. Using this free service, authors can make their results available to the community, in citable form, before we publish the edited article. We will replace this *Accepted Manuscript* with the edited and formatted *Advance Article* as soon as it is available.

You can find more information about *Accepted Manuscripts* in the [Information for Authors](#).

Please note that technical editing may introduce minor changes to the text and/or graphics, which may alter content. The journal's standard [Terms & Conditions](#) and the [Ethical guidelines](#) still apply. In no event shall the Royal Society of Chemistry be held responsible for any errors or omissions in this *Accepted Manuscript* or any consequences arising from the use of any information it contains.



Journal Name

COMMUNICATION

Vibrational Spectroscopy and Imaging for Concurrent Cellular Trafficking of Co-localized Doxorubicin and Deuterated Phospholipid Vesicles

Received 00th January 20xx,
Accepted 00th January 20xx

DOI: 10.1039/x0xx00000x

www.rsc.org/

S. K. Misra,^{a,†} P. Mukherjee,^{b,†} A. Ohoka,^a A. S. Schwartz-Duval,^a S. Tiwari,^b R. Bhargava^{b,*}
and D. Pan^{a,*}

Simultaneous tracking of nanoparticles and encapsulated payload is of great importance and visualizing their activity is arduous. Here we use vibrational spectroscopy to study the in vitro tracking of co-localized lipid nanoparticles and encapsulated drug employing a model system derived from doxorubicin-encapsulated deuterated phospholipid (dodecyl phosphocholine-d₃₈) single tailed phospholipid vesicles.

Nanoparticles designed for diagnostic and therapeutic applications must overcome a series of barriers to success, which include factors external to the body, challenges in delivery to a local site and cellular uptake to eventually perform their desired function.¹ Particle design to achieve both desired localization and function is key for exploiting designer nanoparticles' potential for biomedical applications. In particular, the precise process of drug availability from nanoparticles within living cells is not yet fully understood. The lack of clarity on drug delivery mechanism^{2a-m} also provides less control on cytoplasmic trafficking.^{3a-c} Studies on using fluorescent probes for mechanistic analysis have demonstrated successes in revealing cellular internalization,^{4a-c} membrane interaction,^{5a-c} endosomal escape^{6a-d} and cytoplasmic distribution of fluorophore conjugated drugs.^{7a-c} However, the mode and extent of membrane interactions, chemistry of endosomal escapes and trafficking of cytoplasmic distributions are yet to be thoroughly investigated. While the static microscopic disposition of the drugs (e.g. doxorubicin) has been measured with fluorescent microscopy, the dynamics

controlling the delivery of the drug and simultaneous tracking of the carrier to the cell membrane, the rate of transfer of compound into the cytosol, the rate of release of the drug within the membranes and the accumulation into the nucleus is unknown. Furthermore, it remains challenging to track delivery and co-localization of drugs lacking inherent fluorescence.

Recently, advances in instrumentation^{8a,b} and analytical methods⁹ have allowed vibrational spectroscopic techniques to present new capabilities for rapidly visualizing both cellular identity and delivered particles and payloads. Since vibrational spectroscopy provides quantitative, reproducible estimates of molecular concentration with the capability to delineate the overall dynamics of drug efficacy at multiple scales within the cell, for example from molecular state of the drug to particle to nucleus. Recent report studied the transport of deuterated cationic lipids in a cellular system by Raman spectroscopy¹⁰ and independently tracked intracellular delivery of doxorubicin using fluorescence spectroscopy.¹¹ However, a technique to study the trafficking of both the carrier and payload is still elusive.

To realize this potential, here we report the development of a diagnostic molecular probe that aids in the delivery of a drug molecule and implement vibrational imaging techniques to follow its release inside the cells. Our design employs lipid vesicles for facile permeation and for fusion mediated transport through cell membranes. This model system consists of multiple signature functionalities for robust detectability with vibrational spectroscopic techniques as well as with an intrinsic fluorescence signal from a chromophoric drug such as doxorubicin (DOX), as shown in Figure 1A. Using this strategy we synthesized and characterized (Figure 1B-G) niosomal vesicles from isotopically labelled lipid molecules (dodecyl phosphocholine-d₃₈) that red-shifts the frequency of the C-H modes to the biologically-silent region of the vibrational spectrum (Figure 1F) and call them Deuto-DOX-NPs. Deuto-DOX-NPs can then be identified and their concentration quantified without significant interference from cells with native biological spectra, while the encapsulated DOX

^a Departments of Bioengineering and Materials Science and Engineering, Beckman Institute for Advanced Science and Technology, University of Illinois at Urbana-Champaign, Carle Foundation Hospital, 502 N. Busey St., Urbana, IL 61801, USA, E-mail: dipanjan@illinois.edu

^b Department of Bioengineering, Electrical and Computer Engineering, Chemical and Biomolecular Engineering, Chemistry, and Mechanical Science and Engineering, Beckman Institute for Advanced Science and Technology; University of Illinois at Urbana-Champaign, 1304 W. Springfield Ave, Urbana, IL 61801, USA, E-mail: rxb@illinois.edu

† Authors of equal contribution.

Electronic Supplementary Information (ESI) available: [Raman and confocal images of the Deuto-DOX-NPs in cells, materials and details of methods]. See DOI: 10.1039/x0xx00000x

fluorescence allows for intracellular tracking. For comparative studies, DOX loaded dodecyl phosphocholine single tailed phospholipid vesicles (Lipid-DOX-NPs) were also devised. Deuto-DOX-NPs and Lipid-DOX-NPs were prepared by freeze-thaw-sonication procedure with or without the incorporation of DOX ($1\text{mg}\cdot\text{mL}^{-1}$) in dodecyl phosphocholine-d38 and dodecyl phosphocholine, respectively (details in supporting information).

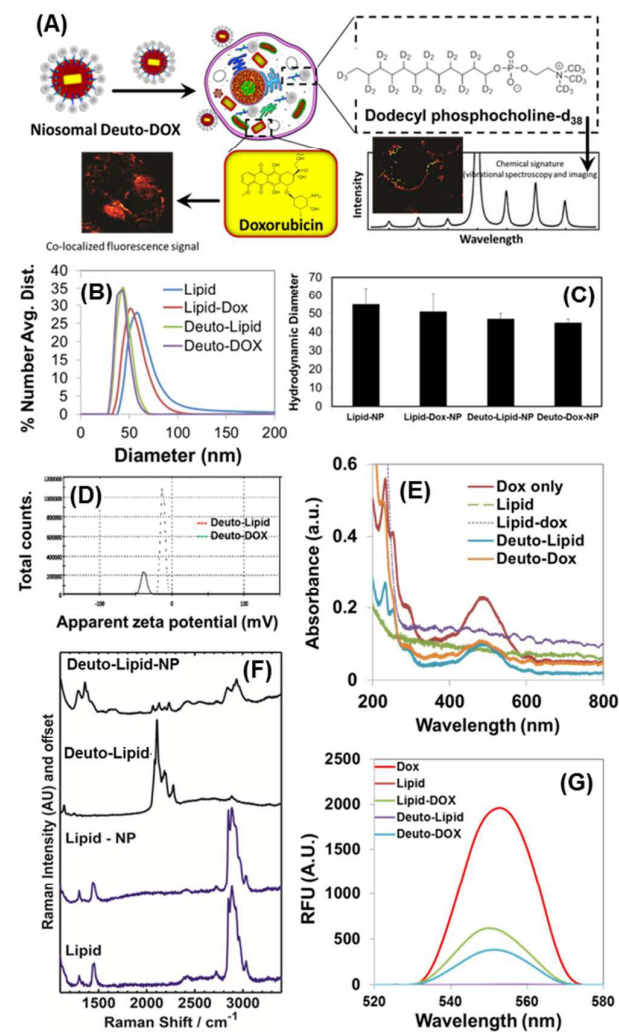


Figure 1. (A) Schematic of the study of synchronized cellular trafficking of co-localized DOX and deuterium-labeled SINGLE TAILED PHOSPHOLIPID VESICLES using vibrational spectroscopy and imaging techniques. Physico-chemical characterization NPs via (B) distribution of diameters, (C) hydrodynamic diameter; (D) zeta potential distribution; (E) UV-Vis absorption spectroscopic signatures; (F) Raman spectra, and (g) fluorescence emission spectra ($\lambda_{\text{ex}} = 450\text{ nm}$) of the formulations.

Incorporation of DOX did not result in a significant variation in hydrodynamic diameter of optimally loaded Deuto-DOX-NPs ($D_{\text{av}} = 45 \pm 02\text{ nm}$) and blank particles Deuto-Lipid-NPs ($47 \pm 03\text{ nm}$). Similarly Lipid-DOX-NPs (non-labelled)

were found to be sized $51 \pm 10\text{ nm}$ compared to blank lipid particles of $55 \pm 09\text{ nm}$. It was noticed that presence of deuterium decreased the size of single tailed phospholipid vesicles with or without loaded DOX, to a very small extent. During the formation of lipid based vesicles, hydrophilic head groups were known to play major role in hydrating the lipid layers and holding the head groups together with involvement of hydrogen bonded layer of hydration. It is known in the literature that hydrogen bonding plays important role in deciding the physical characteristics of lipid assemblies.^{12a,b} The relative hydrogen bonding of deuterium is weaker for molecules associating in a non-H bonding solvent, although the second effect may also be important in aqueous solutions.¹³ This presumably implies that there is lesser number of deuto-lipids in self assembled single tailed phospholipid vesicles leading to a smaller overall hydrodynamic diameter. The overall size reduction effect is however not drastic, possibly due to the absence of appropriately positioned heteroatom in dodecyl phosphocholine capable of forming hydrogen bonds. Representative electrophoretic potential (ζ , surface charge) varied from $-35 \pm 05\text{ mV}$ in case of Deuto-lipid-NPs to $-15 \pm 05\text{ mV}$ after loading of DOX indicating plausible interactions between head group of deuto-lipid and hetero-atom functionalities present in the drug molecule. These interactions were further established by UV-Vis spectroscopic measurements using duplex plasmid DNA (Figure 1E). DNA intercalation ability of DOX was used as deciding factor in interaction measurements revealing decrease in absorbance at $\lambda = 486\text{ nm}$ of DOX and increased for DOX intercalated DNA at $\lambda = 252\text{ nm}$ after interaction with Deuto-DOX or Lipo-DOX. As expected, the formulations without DOX loading could only influence the absorbance at $\lambda = 252\text{ nm}$ due to change in absorption value of duplex DNA.

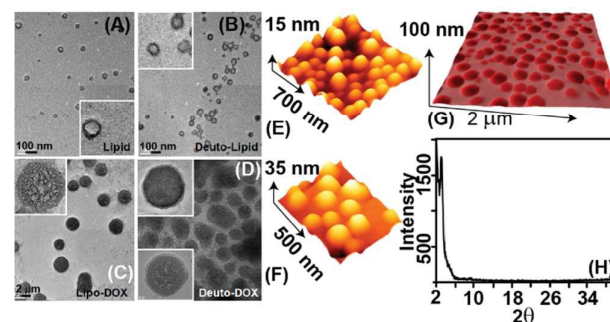


Figure 2. 2D morphology characterization of DOX-loaded SINGLE TAILED PHOSPHOLIPID VESICLES and controls. TEM sample negatively stained by uranyl acetate for (A) lipid, (B) deuto-lipid, (C) lipo-dox and (D) deuto-dox nanoparticles. 3D morphology of (E) deuto-lipid, (F) lipo-dox and (G) deuto-dox nanoparticles. (H) X-ray diffraction pattern of deuto-dox.

Overlaid Raman spectra in Figure 1f showed spectroscopic features of neat lipid and Lipid-DOX-NPs as harmonized but Deuto-DOX-NPs exhibited noticeably weaker $\nu\text{C-D}$ ($2049\text{--}2250\text{ cm}^{-1}$, Figure 1f) Raman intensity. DOX loading is apparent in new features corresponding to the C=C stretch and phenolic groups (C-O) that appear in IR spectra (Figure 5f) but are

overwhelmed by the strong DOX fluorescence (Figure 1G) in Raman measurements. The successful incorporation of DOX was also verified by fluorescence spectroscopic studies. The fluorescence intensity of DOX varied significantly between free and nano-encapsulated state. Relative fluorescence intensity of DOX was found to decrease upon loading in vesicles in both Deuto-DOX and Lipo-DOX (Figure 1G). Vesicles without DOX did not show any significant fluorescence.

2D size distributions of vesicles, both with and without DOX loading, were studied by transmission electron microscopy (TEM) (Figure 2A-D) and 3D profiles were investigated by atomic force microscopy (AFM) (Figure 2E-G). Anhydrous Deuto-lipid particle height grew from 32 ± 06 nm to 40 ± 03 nm in case of Deuto-DOX, while 25 ± 06 nm lipid NPs grew to 28 ± 07 nm for Lipo-DOX. X-ray diffraction studies to investigate the niosomal vesicular structure showed that Lipid particles had a d spacing of 27.9 \AA that confirms a uni-lamellar arrangement (Figure 2H). No significant change was noticed for other NPs (data not shown).

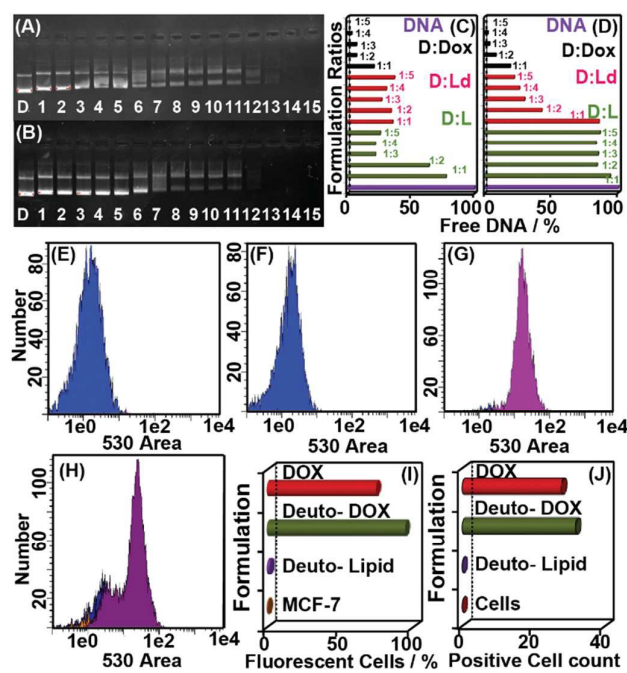


Figure 3. Gel electrophoresis of plasmid DNA incubated with (A) Lipid (Lane 1-5); Lipo-DOX (Lane 6-10) and DOX alone (Lane 11-15) (B) Deuto-Lipid (Lane 1-5); Deuto-DOX (Lane 6-10) and DOX alone (Lane 11-15). Quantification of retarded plasmid DNA incubated with (C) Lipid; Lipo-DOX and DOX alone and (D) Deuto-Lipid; Deuto-DOX and DOX alone. Experiments were performed at ratios ranging from 1:1 to 1:5. (E-H) Cell internalization histograms obtained from FACS analysis on (E) cells alone and treated with 0.1 mg/mL of (F) Deuto-Lipid; (G) Deuto-DOX; (H) DOX alone; (I) summary of % cell population and (J) comparison of DOX positive cell count calculated from fluorescence microscopy

Encapsulation of DOX in formulations of Deuto-DOX-NPs and Lipid-DOX-NPs were studied by their interaction with duplex DNA in agarose gel under the influence of electrophoretic mobility (Figure 3A-B). Both formulations were found to interact similarly with duplex DNA with no significant difference in % DNA binding but were markedly different from DOX alone. Compared to $\sim 100\%$ DNA gel retardation by DOX at ratio of 1:5 (DNA:DOX), Deuto-DOX and Lipo-DOX achieved ~ 70 and 60% , respectively. In contrast, control lipid vesicles interacted more with duplex DNA compared to Deuto-Lipid (~ 70 vs. 20% DNA binding in Figure 3c and d). To visualize the release of DOX inside cells, fluorescence imaging and flow assisted cell sorting assays (FACS) were performed on human breast adenocarcinoma cells (MCF-7 cell line). FACS analysis of untreated cells (Figure 3E) and treated with Deuto-Lipid only (Figure 3F) did not show any cell population with extra fluorescence above the non-specific cell background. In sharp contrast, $\sim 95\%$ of cells treated with Deuto-DOX-NPs showed a positive response (Figure 3G) while only $\sim 70\%$ of free-DOX treated cells were positive, as summarized in Figure 3H. Cellular internalization, visualized by fluorescence imaging, was achieved in a significant population of cells treated with Deuto-DOX and free DOX. On the other hand, untreated cells or cells treated with deuto-Lipid did not show any noticeable increase in background fluorescence of cells (Figure 3I-J).

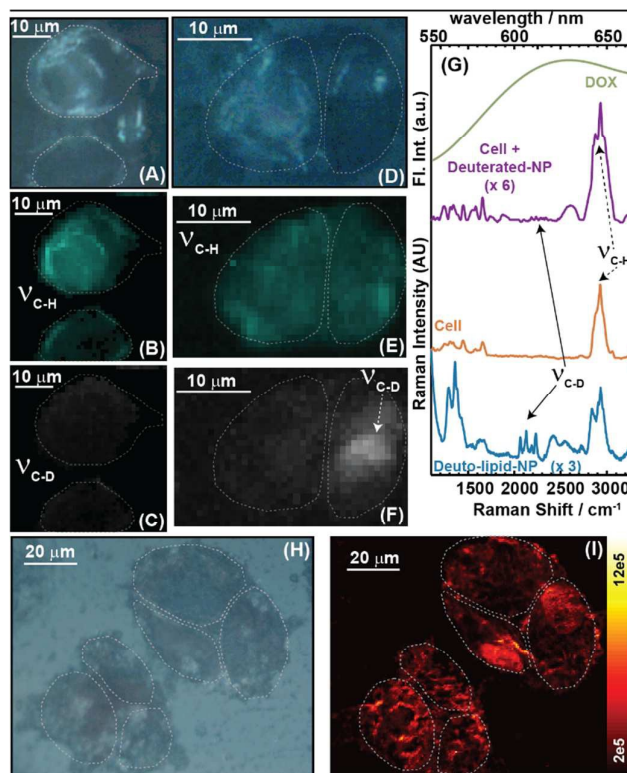


Figure 4. (A) Bright field and Raman intensity maps at (B) $2922 \text{ (}\nu\text{C-H) cm}^{-1}$ and (C) $2230 \text{ (}\nu\text{C-D) cm}^{-1}$ of untreated breast cancer cells. (D), (E) and (F) show the same images except the cells are treated with Deuto-Lip-NPs. (G) DOX fluorescence and

the average Raman spectra from native and drug treated cells and nanoparticles. (H) Representative bright field image and fluorescence image (I) of the DOX treated breast cancer cells.

After establishing the integrity of Deuto-DOX-Lipid vesicles, and their cell internalization efficiencies, we resorted to Raman spectroscopic imaging to estimate abundance and visualize distribution of Deuto-lipid and DOX in cells. Shown in Figure 4 are the (A, B) optical brightfield and Raman images of MCF cells with no nanoparticles. Raman intensities were measured by plotting the ν -CH (B) and ν -CD (C) bands at 2230 cm^{-1} . Since there were no spectroscopic features at the ν -CD region of the cells, image 4C results from scattering of the incident laser light. In comparing corresponding images obtained from Deuto-Lipid treated cells using the same analyses, we noted a significant change in the image pattern. In Figure 4 E and F, measured similar to B and C, the image based on ν -CH intensity outlines the cells while ν -CD image shows the presence of the Deuto-Lipid. In comparison, when only DOX was incubated with the cells, we observed a significant fluorescence contribution (Figure 4 I), that was integrated from a 2nd polynomial fit to the spectra. DOX was found to be distributed in no particular pattern in the cell. For clarity the bright field images corresponding to each of these measurements are displayed in A, D and H. The spectral properties of cells and the nanoparticles are summarized in Figure 4G, which shows comparative spectra and changes in treated cells as expected.

To address the stability of DOX inside vesicles of Deuto-Lipids, Raman images from blank cover slides, and dry Deuto-DOX deposited on cover slides were measured. Figure 5(A) showed the fluorescence image of the Deuto-DOX on the coverslips, while the inset displays the same image from the blank cover slip. Figure 5(B) and (C) display the Raman images corresponding to the intensities obtained at 2250 cm^{-1} (ν -CD) and 1260 cm^{-1} (drug), with the insets displaying the Raman image from the blank cover slips. Since the drug fluorescence interferes with the ν -CD region, complementary infrared spectroscopic images of the same were acquired that are shown in (D) and (E). Also a protocol was followed, as mentioned in the supplementary section to de-convolute the fluorescence from the C-D Raman spectra. For each of the conditions, the images were subjected to the analysis mentioned above. We note distinct spectral features arising in the $2150\text{--}2350\text{ cm}^{-1}$ region that is characteristic of the C-D vibrations as evidenced in the Deuto-lipid nanoparticles (Figure 1F), while they are absent in the average spectrum of the cell. For the Raman spectra of Cellular matrix with Deuto-DOX-NP, we observe a characteristic peak of the C-D stretch at four wavelengths 2187 cm^{-1} , 2220 cm^{-1} , 2300 cm^{-1} and 2320 cm^{-1} (Figure S3, cyan). Both the images (D and E) point to the presence of drug and Deuto-lipids in the same region. Thus the stability of the drug within the lipid nanoparticles and its co-localization with the same was ascertained. Figure 5F shows the average infrared spectra of the bare and DOX loaded Deuto-lipid nanoparticles and the ν - ν CD peaks are highlighted in (F1).

For Deuto-DOX treated cells, Figure 5G displays the bright field, while H plots the D-lipid-NPs, DOX and cellular distribution in a single image. The individual contributions are displayed separately in (I-K) that is measured in a similar fashion as in Figure 4. These observations point to the presence of DOX and the lipid NPs in the same region. Presence of cellular regions is displayed in panel J, which results from the pixels with intensity at the amide I region after proper baselining was achieved to eliminate fluorescence contributions. Regions corresponding to the intensity corresponding to the Deuterium species (2230 cm^{-1}) fill up the partial void in panel K and implies the presence both cellular species and lipid nanoparticles. Select region as pointed out in (H) has all the three contributions: cellular, D-Lipid NPs and DOX. A significant overlap between the DOX and D-lipid-NPs can be noticed that can account for the co-localization of the drug with the nanoparticles, while the separated region (red) points to the drug released region.

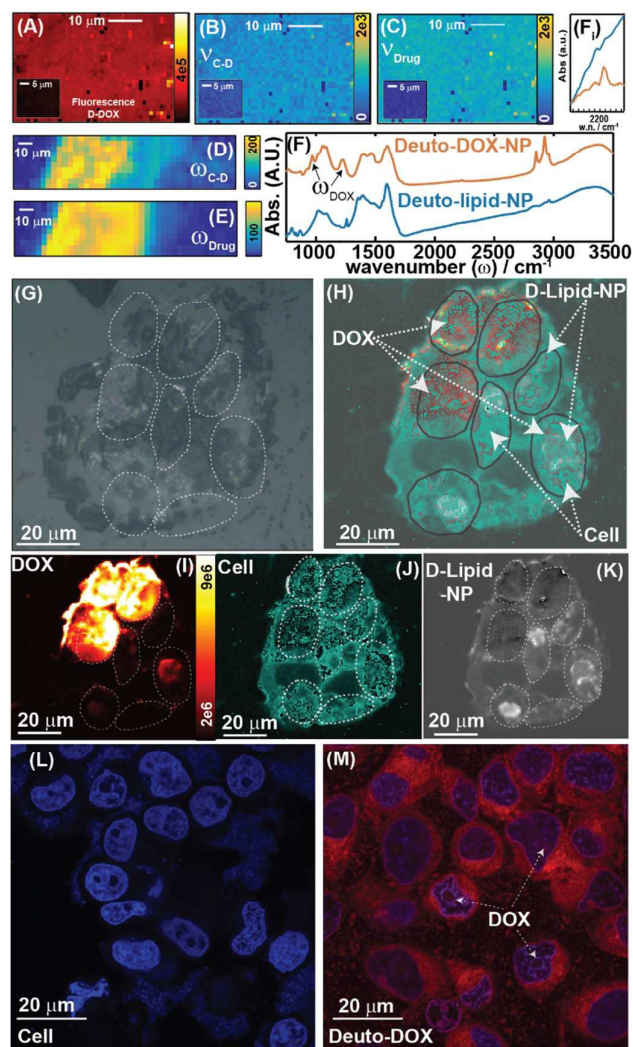


Figure 5. (A), (B) and (C) fluorescence, Raman images of the Deuto-DOX-NPs. Insets show the images corresponding to a

blank coverslip. (F) compares the IR spectra of Deuto-lipid-NPs to the Deuto-DOX-NPs and we isolate spectral regions corresponding to the drug and nanoparticle. (D) and (E) display the intensity profile corresponding to the drug and lipids for Deuto-DOX-NPs after drying on a low E slide. (G-K) displays the fluorescence and Raman images of cells treated with Deuto-DOX-NPs at different conditions discussed in the text. H is the collective image of I, J and K taken together; (L) and (M) shows the fluorescence confocal images of cells without and with Deuto-DOX respectively.

Finally, the functional ability of loaded DOX was verified in two breast cancer cell lines, namely MCF-7 and MDA-MB231. Formulations were delivered in cells and incubated for 42h before visualizing under microscope to evaluate the effect of DOX on cell growth density and morphology. A significant loss of cell growth density was reported in MCF-7 cells treated with Deuto-DOX (Figure 6B) and free DOX (Figure 6C) compared to untreated cells (Figure 6A) while vesicles from Deuto-lipids (Figure 6D) did not show any particular variation. An MTT assay showed the effects of various treatments on MCF-7 (Figure 6E) and MDA-MB231 cells (Figure 6F). While MCF-7 cells are tumorigenic, MDA-MB231 display strong characteristics of metastatic disease, likely explaining the difference in behaviour that we observe.

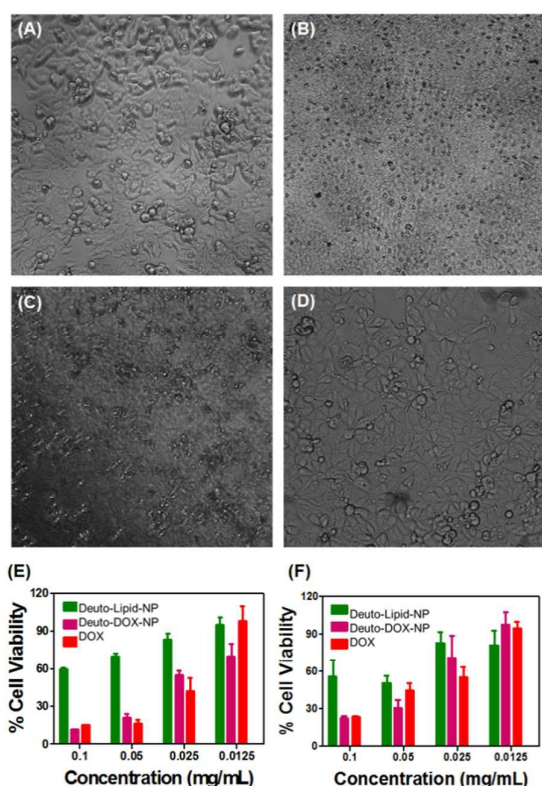


Figure 6. Growth regression analysis on treated cells. Bright field image of MCF-7 cells (A) untreated and treated with 0.1 mg/mL of (B) Deuto-DOX; (C) DOX and (D) Deuto-lipid. Viability

assay on MCF-7 (E) and MDA-MB231 (F) at various concentrations of the used formulation.

A similar observation can be made for regions with smaller intensity ratios of the ν -CH to ν -CD (< 0.5) surrounding the DOX and highlighted in Figure S2, which could result from the release of the DOX from the Deuto-Lipid vesicles. Conventional methods of tracking and visualizing drug internalization are greatly dependent on fluorescence confocal based techniques, where the success of the method is heavily relied on the intrinsic fluorescence of the drug (e.g. DOX). The interference of the DOX fluorescence with the C-D vibrational mode is clearly evident in the Raman spectra and select protocols if properly implemented can de-convolute the Raman spectra of the particles from the fluorescence as evident in Figure S3 (supplementary section), outlining the C-D spectra in the 2100-2400 cm^{-1} ranges and identifying the peak that was used to plot the intensity maps. Fluorescence confocal results substantiates the internalization and nuclear abundance of DOX fluorescence (red) as evident in and around nucleus of the cells stained with DAPI (blue). (Figure 5L-M). However, we demonstrate for the first time that for drug molecules with low or no inherent fluorescence, vibrational spectroscopic techniques would be a great choice for their intracellular tracking. To avoid thermal oscillations in the spectra, low-E slides were used to acquire Raman spectra. As evident, the Raman intensities of the C-D modes are low, but discernible. Future imaging applications are going to be addressed with Stimulated Raman measurements.

Conclusions

In summary, we designed a model system to study intracellular trafficking of nanoparticles and encapsulated drug. The system showed well defined morphology with stable nano-suspension in aqueous medium. Deuto-DOX was found to have a monolayered structure with encapsulated DOX, which was verified by x-ray diffraction, spectroscopic, imaging and FACS analyses. Spectroscopic imaging studies revealed the co-localization of DOX and deuterated lipid molecules inside cellular cytoplasm with finer details. It was also established that loaded DOX was functionally active in breast cancer cells to significantly reduce cancer cell growth with loss in growth density and morphology. In conclusion, Deuto-dox-NPs are designed as a model system to study simultaneous trafficking of drugs and their carriers. We report a successful strategy of identifying the carrier molecules with vibrational spectroscopy followed by plausible tracking of the release of payload within the cells. Tracking of drugs and function can be widely applicable to several other drugs with same or other carrier agents with feasibility of being deuterated.

Notes and references

We thank Dr. Tor Jensen for help with the FACS analysis. TEM, AFM and zeta potential experiments were carried out at

Frederick Seitz Materials Research Laboratory Central research facilities, UIUC. The research was partly supported by the National Institutes of Health via grant R21CA190120, University of Illinois and Children Discovery Institute.

- 1 a) X. Gao, L. Huang, *Biochim. Biophys. Res. Commun.*, 1991, **179**, 280; b) S. K. Misra, M. Ye, S. Kim, D. Pan, *Chem. Commun.*, 2014, **50**, 13220; c) S. Hasegawa, N. Hirashima, M. Nakanishi, *Bioorg. Med. Chem. Lett.*, 2002, **12**, 1299; d) M. Nakanishi, *Curr. Med. Chem.* 2003, **10**, 1289–1296; e) S. K. Misra, J. Kus, S. Kim, D. Pan, *Mol. Pharm.*, 2014, **11**, 4218; f) A. Wicki, D. Witzigmann, V. Balasubramanian, J. Huwyler, *J. Contr. Rel.*, 2015, **200**, 138-157; g) S. Mura, D. T. Bui, P. Couvreur, J. Nicolas, *J. Contr. Rel.*, 2015, **208**, 25; h) J. Nicolas, S. Mura, D. Brambilla, N. Mackiewicz, P. Couvreur, *Chem. Soc. Rev.*, 2013, **42**, 1147; i) M. ElSabahy, K. L. Wooley, *Chem. Soc. Rev.*, 2012, **41**, 2545; j) S. K. Misra, M. Ye, S. Kim, D. Pan, *PLoS ONE*, 2015, **10**, e0125908; k) Y. Bae, K. Kataoka, *Adv. Drug Deliv. Rev.*, 2009, **61**, 768; l) P. Mukherjee, S. K. Misra, M. C. Gryka, H.-H. Chang, S. Tiwari, W. L. Wilson, J. W. Scott, R. Bhargava, D. Pan, *Small*, 2015, DOI: 10.1002/smll.201500728; m) S. K. Misra, T. W. Jensen, D. Pan, *Nanoscale*, 2015, **7**, 7127.
- 2 a) M. Paranjpe, C. C. Müller-Goymann, *Int. J. Mol. Sci.*, 2014, **15**, 5852; b) P. T. Wong, S. K. Choi, *Chem. Rev.*, 2015, **115**, 3388.
- 3 a) R. Misra, S. K. Sahoo, *Eur. J. Pharm. Sci.*, 2010, **39**, 152; b) P. L. Paine, L. C. Moore, S. B. Horowitz, *Nature*, 1975, **254**, 109; c) N. Pante, M. Kann, *Mol. Biol. Cell*, 2002, **13**, 425.
- 4 a) I. Maeger, E. Eiriksdottir, K. Langel, S. El Andaloussi, U. Langel, *Biochim. Biophys. Acta, Biomem.*, 2010, **1798**, 338; b) W. B. Edwards, W. J. Akers, Y. Ye, P. P. Cheney, S. Bloch, B. Xu, R. Laforest, S. Achilefu, *Mol. Imag.*, 2009, **8**, 101; c) W. Chun; T. Fu; W. Xiaoyu; L. Lidong, *ACS Appl. Mater. Inter.*, 2015, **7**, 13653.
- 5 a) W. Cho, R. V. Stahelin, *Ann. Rev. Biophys. Biomol. Struct.*, 2005, **34**, 119; b) B. Daniel; H. Harald; F. Jamie; F. Andrew, *Mol. Cell. Prot.: MCP*, 2006, **5**, 2175; c) W. Cho, R. V. Stahelin, *Ann. Rev. Biophys. Biomol. Struct.*, 2005, **34**, 119.
- 6 a) R. N. Majzoub, C-L. Chan, K. K. Ewert, B. F. B. Silva, K. S. Liang, C. R. Safinya, *Biochim. Biophys. Acta, Biomem.*, 2015, **1848**, 1308; b) D. P. Morales, G. B. Braun, A. Pallaoro, R. Chen, X. Huang, J. A. Zasadzinski, N. O. Reich, *Mol. Pharm.*, 2015, **12**, 600; c) A. Erazo-Oliveras, N. Muthukrishnan, R. Baker, T-Y. Wang, J-P. Pellois, *Pharmaceuticals (Basel)*, 2012, **5**, 1177; d) B. R. Liu, S-Y. Lo, C-C. Liu, C-L. Chyan, Y-W. Huang, R. S. Aronstam, H-J. Lee, *PLoS ONE*, 2013, **8**, e67100.
- 7 a) J. O. Escobedo, Y-H. Chua, Q. Wang, P. S. Steyger, R. M. Strongin, *Nat. Prod. Commun.*, 2012, **7**, 317; b) R. Fischer, T. Waizenegger, K. Köhler, R. Brock, *Biochim. Biophys. Acta*, 2002, **1564**, 365; c) S. S. Agasti, A. M. Laughney, R. H. Kohlera, R. Weissleder, *Chem. Commun.*, 2013, **49**, 11050.
- 8 a) W. Min, C. W. Freudiger, S. Lu, X. S. Xie, *Ann. Rev. Phys. Chem.*, 2011, **62**, 507; b) R. Bhargava, *Appl. Spectrosc.*, 2012, **66**, 1091.
- 9 D. Mayerich, M. J. Walsh, A. Kadjacsy-Balla, P. S. Ray, S. M. Hewitt, R. Bhargava. *Technology (Singap World Sci)*, 2015, **3**, 27.
- 10 T. Chernenko, R. R. Sawant, M. Miljkovic, L. Quintero, M. Diem, and V. Torchilin, *Mol. Pharm.*, 2012, **9**, 930.
- 11 A. L. B. Seynhaeve, B. M. Dicheva, S. Hoving, G. A. Koning, T. L. M. ten Hagen, *J. Control. Rel.*, 2013, **172**, 330.
- 12 (a) E. Diamanti, L. Cuellar, D. Gregurec, S. E. Moya, E. Donath, *Langmuir*, 2015, **31**, 8623; (b) S. K. Misra, J. Biswas, P. Kondaiah, S. Bhattacharya, *PLoS ONE*, 2013, **8**, e68305.
- 13 A. Grimiso, *J. Phys. Chem.*, 1983, **67**, 962.